Pseudopotential band calculations along a symmetry axis: spin-orbit interaction

1994 J. Phys.: Condens. Matter 6 4673

(http://iopscience.iop.org/0953-8984/6/25/006)

J. Phys.: Condens. Matter 6 (1994) 4673–4684. Printed in the UK

Pseudopotential band calculations along a symmetry axis: spin–orbit interaction

D Agassi and J B Restorff
Naval Surface Warfare Center, Silver Spring, MD 20903-5000, USA

Received 26 January 1994

Abstract. A convergent method for local pseudopotential band structure calculations, based on a cylindrical coordinate multipole expansion, is generalized to include the spin–orbit interaction. The generalization is necessary for systems that are highly anisotropic and where the spin–orbit interaction is essential, e.g., narrow-gap semiconductor superlattices. The coupled wave equations for the corresponding multipoles are derived and applied to a test case: the low bands of PbSe along the [111] direction. The calculated bands compare well with the PbSe band structure.

1. Introduction

In a previous paper [1] (hereafter referred to as I) we introduce a method for local pseudopotential band structure calculations along a symmetry axis. The method consists of expanding the wavefunction and pseudopotential in cylindrical coordinate multipoles, where the cylindrical coordinate system is chosen such that its z-axis coincides with the symmetry axis. Correspondingly, the three-dimensional Schrödinger equation is transcribed into a coupled set of *one-dimensional* wave equations for the multipoles. The method is expected to be advantageous for anisotropic systems such as epitaxial semiconductor superlattices and interfaces, where a particular direction in space is of special significance. The good convergence properties of the method are demonstrated in I for a test case. The objectives of this paper are to generalize the above method to include the spin–orbit (SO) interaction, and demonstrate its implementation for a simple test case. This generalization is necessary in situations where the SO interaction plays an essential role and the structure is anisotropic. A case in point is the technologically important layered structure of heavy-element narrow-gap semiconductors of the II–VI, IV–VI [2] and III–V systems. Since the SO splitting and band gap are comparable for these semiconductors [3], it is necessary to include the SO interaction for a realistic description of the small band gap. Other possible applications are magnetic layered structures [4] where the SO and other spin interactions constitute an essential part of the physics, and g-factor calculations [5] for which the SO interaction and spin degrees of freedom are indispensable. It should be emphasized that although the non-scalar SO interaction in these examples is essential for some aspects of the calculation, it is in general too weak to substantially 'renormalize' the central pseudopotential. Consequently, the effects considered here consist of SO admixtures of the central potential bands.

At the core of the method is a cylindrical multipole expansion of lattice periodic functions. As an example consider a spinless band wavefunctions $\Psi(\boldsymbol{r}')$, where the crystal's momentum $\boldsymbol{k}$ points along the symmetry axis direction. The corresponding cylindrical

0953-8984/94/254673+12$19.50

multipole expansion is [1]

$$\Psi(r') = \sum_{g_F} \sum_{l=-\infty}^{\infty} \Psi_l(g_F, z') J_l(g_F \rho) e^{il\phi}. \tag{1.1}$$

In (1.1) and hereafter primed variables refer to the cylindrical coordinate system chosen such that its z-axis (z') coincides with the symmetry axis. The g_F index runs over a lattice-specific non-negative series (see table 1 for an FCC lattice), $J_l(x)$ is the Bessel function of order l [6] and (ρ, ϕ, z') are the standard cylindrical coordinates. Good convergence of (1.1) implies that a small number of distinct multipoles $\Psi_l(g_F, z')$ suffices for a good description of the $\Psi(r')$ functions corresponding to low bands.

Table 1. The lowest g-values and $\Phi_0(g)$ angle (3.1) for the PbSe (FCC) lattice in the [111] direction [1] and $g = f/a$ (Å).

f	g(PbSe)[a] (Å^{-1})	$\Phi_0(g)$ (°)
0	0	0
$10.2606 = 2\pi\sqrt{\frac{8}{3}}$	1.6754	0
$17.7714 = 2\pi\sqrt{8}$	2.9018	30
$20.5207 = 2\pi\sqrt{\frac{32}{3}}$	3.3507	0
27.1465	4.4326	19.1066
30.7813	5.0261	0
35.5430	5.8036	30
36.9944	6.0406	13.8979

[a] We used a(PbSe, T = 300 K) = 6.1243 Å.

The convergence of (1.1) hinges on two general properties, which severely limits the number of contributing l and g_F indices. The l-sequence is controlled by the symmetry of the z'-axis. For example, group theoretic considerations imply that for an FCC lattice and $\hat{z}' \| [111]$ only *two* l values need be considered. All other multipoles are phase related to those two multipoles [1]. As a consequence, expansion (1.1) is in effect an expansion in g_F. The g_F expansion, in turn, is controlled by an energy–geometry consideration. To elaborate on this, note that the transverse behaviour of $\Psi(r')$ is controlled by the oscillations of $J_l(g_F\rho)$, with a period g_F^{-1} [6]. Therefore, for 'low' bands, the important terms in (1.1) involve the lowest g_F-values up to a 'small' cut-off value g_c. For the [111] direction in particular, the latter has been estimated in I to satisfy $(l_m + \frac{3}{2})/g_c \simeq 0.5a_T$ where l_m is a 'typical' l-value and a_T is approximately the lattice constant in the *transverse direction*. Thus both the l and the g variations in expansion (1.1) are severely restricted, hence the good convergence. Note that the above considerations are valid regardless of the extension of the unit cell in the $\hat{z}'$ direction. Thus expansion (1.1) is expected to become advantageous for structures where the unit cell extension in the z'-direction is large, such as in superlattices. Another important feature of the method is the simplicity of the coupled set of wave equations for the multipoles. The pertaining coupling potentials are derived from the underlying three-dimensional local pseudopotential by means of geometrical coefficients—the 'A-coefficients' [1] (see section 4). These coefficients control the transverse reciprocal lattice momentum addition.

With the SO interaction included, the above features hold true though the details change considerably. The main complication is that the spin wave function is comprised of two

components, pertaining to the two possible spin projections. Consequently two multipole expansions such as (1.1) need to be considered simultaneously and the total number of relevant multipoles roughly doubles. Correspondingly, the coupled set of wave equations for the multipoles (4.2), includes new spin terms.

To demonstrate the implementation of the method we consider the band structure of PbSe along the [111] direction. This narrow-gap semiconductor without SO has been studied in I, and a convergent multipole basis set has been established. The present PbSe calculation shows that given a correct description of the central potential bandstructure, the spin-generalized multipole wave equation (4.2) yields the correct bands. The analysis also demonstrates how group theoretic considerations determine the SO admixtures and the effect of band gap reduction by the SO interaction.

The paper is organized as follows. In section 2 we introduce the multipole expansion in the presence of spin and in section 3 we discuss symmetry properties pertaining to the cylindrical multipole expansion. The derivation of the wave equations for the multipoles is outlined in section 4. The last section contains the results of PbSe band structure calculations along the Γ–L direction and a brief discussion. The technical details omitted here are given elsewhere [7].

2. Cylindrical coordinate multipole expansions

The spinor Bloch function in the unprimed coordinates ($\Psi_{nk}(r)$) has the form

$$(\Psi_{nk}(r)) = e^{ik\cdot r}(U_{nk}(r)) = \sum_{\sigma=\pm 1} e^{ik\cdot r} U_{nk}^{(\sigma)}(r)(\chi(\sigma)) = \begin{pmatrix} U_{nk}^{(+)} & (r) \\ U_{nk}^{(-)} & (r) \end{pmatrix} \quad (2.1)$$

where hereafter parentheses $(\ldots)$ denote a spinor, and $U_{nk}^{(\sigma)}(r)$ is a lattice periodic function [8]. To obtain the multipole expansion of (2.1) it is first transformed to the primed coordinates using [9]

$$\hat{R}[\Phi(r)(\chi)] = [\hat{R}\Phi(r)][\hat{R}(\chi)] \quad (2.2)$$

where $\hat{R}$ is the rotation operator, and $\Phi(r)$ and (χ) are an arbitrary function and spinor, respectively. The spinor factor $[\hat{R}(\chi)]$ transforms according to the $D^{1/2}(\alpha, \beta, \gamma)$ two-dimensional matrix [9, 10], where α, β, and γ are the Euler angles, and the radial factor $[\hat{R}\Psi(r)] = \Psi(\hat{R}^{-1}r')$ has been discussed in I. Limiting ourselves, as in I, to crystal momenta k' such that $k \cdot r = k' \cdot r' = k'z'$, the wavefunction in the primed coordinates is

$$(\Psi_{nk'}(r')) = e^{ik'z'} \sum_{\sigma=\pm 1} U_{nk'}^{(\sigma)}(r')(\chi'(\sigma)) \quad (2.3)$$

where the [111]-projected crystal momentum k' is

$$k' = K3\pi/a^* \qquad a^* = a\sqrt{3} \qquad 0 < K \leqslant 1. \quad (2.4)$$

The wavefunction spinor (2.3) entails two lattice periodic functions. Consequently, the steps in section 2 of I yield the multipole expansion

$$(\Psi_{nk'}(r')) = \sum_{\sigma=\pm 1} \sum_{g_F} \sum_{l=-\infty}^{\infty} \Psi_l^{(\sigma)}(g_F, z') J_l(g_F \rho) e^{il\phi}(\chi'(\sigma)) \quad (2.5a)$$

where the spin multipoles are given by

$$\Psi_l^{(\sigma)}(g_F, z') = i^l \sum_{L':|L'_T|=g_F} \Psi^{(\sigma)}(L') e^{i(k'+L'_z)z'} e^{-il\delta(L'_T)} \tag{2.5b}$$

L' denotes a reciprocal lattice vector, L'_T its transverse component (normal to z'), $\Psi(L')$ are the Fourier coefficients of $\Psi(r')$ and the shift phase $\delta(L'_T)$ is defined in I. The summation in (2.5*b*) is over all L' such that $|L'_T| = g_F$.

We turn now to the SO interaction. The standard 'atomic' form is $\zeta(r)(\sigma \cdot l)$ [11], where $\sigma = (\sigma_x, \sigma_y, \sigma_z)$ is the Pauli matrix vector and $l = -ir \times \nabla$. For a lattice periodic array of ions at r_i the SO interaction takes the form

$$(\hat{V}_{SO}(r)) = \sum_i \zeta_i(|r - r_i|)(\sigma \cdot l_{(r-r_i)}) = -i\sigma \cdot (f(r) \times \nabla) \tag{2.6}$$

where the lattice periodic SO vector form factor $f(r)$ is

$$f(r) \equiv \sum_i \zeta_i(|r - r_i|)(r - r_i) = \sum_G f(G) e^{iG \cdot r}. \tag{2.7}$$

When expressed in this form, the transformation of (2.6) to the primed coordinates is straightforward since all factors on the LHS of (2.6) are invariant under rotation. Consequently (2.6) and (2.7) are valid in the primed coordinates provided that all factors are replaced by their primed counterparts. The form of the RHS of (2.6) is mathematically convenient to apply on products of the form $\exp(iG' \cdot r')(\chi'(\sigma))$ that enter the calculation.

Since the vector form factor defined in (2.7) is lattice periodic, it has its own multipole expansion:

$$\begin{aligned} f(r') &= \sum_{g_Q} \sum_{l=-\infty}^{\infty} f_l(g_Q, z') J_l(g_Q \rho) e^{il\phi} \\ f_l(g_Q, z') &= i^l \sum_{G':|G'_T|=g_Q} f(G') e^{iG'_z z'} e^{-il\delta(G'_T)}. \end{aligned} \tag{2.8}$$

The multipoles $f_l(g_Q, z')$ of (2.8) (of dimensionality $[E^* l]$) are the SO counterparts of the central pseudopotential multipoles.

3. Symmetry properties

As alluded to in section 1, not all l-values in the multipole expansion, e.g., (1.1), (2.5), are allowed, and not all allowed multipoles are independent [1]. These constraints and relations, which are part and parcel of the basic wave equation (see sections 4 and 5), are discussed here. They are dictated by the symmetry group of the vector k (under which the Hamiltonian is invariant). In the presence of the SO interaction and for the particular [111] direction these are the double groups $C_{3v}^{(d)}$ and $D_{3d}^{(d)}$ for the Λ and L points, respectively [9, 10]. The corresponding allowed l-sequences for the multipoles are given in tables 2 and

Table 2. The Λ-point allowed l-sequences. The corresponding representations of the double group $C_{3v}^{(d)}$ are denoted in the notation of [10]. The upper and lower l-sequences in each spinor correspond to the $\sigma = +1$ and $\sigma = -1$ components, respectively. For one-dimensional representations, $U_l(z')$ and $V_l(z')$ are the z'-dependent factors in the l-expansion of the two components of the basis spinor [7, 9] (analogous to (2.1)). For the two-dimensional representations, $W_l(z')$ and $X_l(z')$ correspond to $U_l(z')$ and $V_l(z')$, respectively, of the second basis spinor.

Irreducible representation	l-values[a]	l-parity $\hat{\pi}_l$ [b]
Λ_4	$\|1\rangle = \begin{pmatrix} 3m-1 \\ 3m+1 \end{pmatrix}$	$(-1)^{3m}\begin{pmatrix} 0 & i \\ -i & 0 \end{pmatrix}$
Λ_5	$\|1\rangle = \begin{pmatrix} 3m-1 \\ 3m+1 \end{pmatrix}$	$-(-1)^{3m}\begin{pmatrix} 0 & i \\ -i & 0 \end{pmatrix}$
Λ_6	$\|1\rangle = \begin{pmatrix} 3m \\ 3m+1 \end{pmatrix}$ $\|2\rangle = \begin{pmatrix} 3m-1 \\ 3m \end{pmatrix}$	$(-1)^{3m}\begin{pmatrix} 0 & 0 & 0 & 1 \\ 0 & 0 & 1 & 0 \\ 0 & 1 & 0 & 0 \\ 1 & 0 & 0 & 0 \end{pmatrix}$

[a] $m = 0, \pm 1, \pm 2, \pm 3, \ldots$.

[b] $\begin{pmatrix} U_{-l}(g, z') \\ V_{-l}(g, z') \end{pmatrix} \equiv \hat{\pi}_l \begin{pmatrix} U_l(g, z') \\ V_l(g, z') \end{pmatrix}$ or $\begin{pmatrix} U_{-l}(g, z') \\ V_{-l}(g, z') \\ W_{-l}(g, z') \\ X_{-l}(g, z') \end{pmatrix} \equiv \hat{\pi}_l \begin{pmatrix} U_l(g, z') \\ V_l(g, z') \\ W_l(g, z') \\ X_l(g, z') \end{pmatrix}$.

3 for the Λ and L points, respectively. Note that the l-sequences for 'up' and 'down' spin components are different, even though all entail ±3 increments.

As in I, the central potential multipoles $v_l(g_P, z')$ satisfy the l-periodicity relation [1]:

$$v_{l\pm 6}(g_P, z') = -e^{\pm 6i\Phi_0(g_P)} v_l(g_P, z') \qquad \text{for } \sin[6\Phi_0(g_P)] = 0 \tag{3.1}$$

and $\Phi_0(g)$ is given in table 1 [1]. When $\sin[6\Phi_0(g)] \neq 0$, the corresponding l-periodicity relationship is more complex; however, for the test case in section 5, (3.1) suffices. As for the SO vector form factor $\boldsymbol{f}(r')$, (2.7), it can be shown [11] that $\boldsymbol{f}(r') = \nabla' V(r')$ where $V(r')$ denotes a central potential with a multipole expansion of the form (1.1) where $l = 0, \pm 3, \pm 6, \ldots$. Consequently, by expressing the gradient operator in cylindrical coordinates and employing properties of the Bessel function [6], the following phase relations among the $\boldsymbol{f}(r) \equiv (f^{(x')}, f^{(y')}, f^{(z')})$ components are obtained:

$$\begin{aligned} f_{3m+1}^{(x')}(g_Q, z') &= -f_{3m-1}^{(x')}(g_Q, z') = i f_{3m+1}^{(y')}(g_Q, z') \\ f_{3m+1}^{(y')}(g_Q, z') &= f_{3m-1}^{(y')}(g_Q, z') = i f_{3m-1}^{(x')}(g_Q, z') \\ f_{3m}^{(z')}(g_Q, z') &\neq 0 \qquad \text{for } m = 0, \pm 1, \pm 2, \ldots. \end{aligned} \tag{3.2}$$

According to table 3 in I the l-sequence in (3.2) implies that $(f_l^{(x')}(z'), f_l^{(y')}(z'))$ and $f_l^{(z')}(z')$ transform as the L_3' and L_2' representations of D_{3d}, respectively.

Comparing the irreducible representations' allowed l-sequences with and without spin, i.e., tables 2 and 3 with tables 2 and 3 in I, readily reveals which zero-spin bands are admixed by the SO interaction, i.e., the compatibility relations [9]. Consider first the case of a Λ-point, i.e. compare table 2 with table 2 in I. By matching the l-sequences it follows that the spinless Λ_1, Λ_2 and Λ_3 representations are admixed to yield the Λ_6 spin representation.

Table 3. The L-point allowed l-sequences. The corresponding representations of the double group $D_{3d}^{(d)}$ are denoted in the notation of [10]. The symbols are explained in the caption of table 2.

Irreducible representation	l-values[a]	l-parity $\hat{\pi}_l$[b]	z-parity $\hat{\pi}_z$[c]
L_4^+	$\|1\rangle = \begin{pmatrix} 3m-1 \\ 3m+1 \end{pmatrix}$	$(-1)^{3m}\begin{pmatrix} 0 & -i \\ i & 0 \end{pmatrix}$	$(-1)^l\begin{pmatrix} 1 & 0 \\ 0 & 1 \end{pmatrix}$
L_5^+	$\|1\rangle = \begin{pmatrix} 3m-1 \\ 3m+1 \end{pmatrix}$	$-(-1)^{3m}\begin{pmatrix} 0 & -i \\ i & 0 \end{pmatrix}$	$(-1)^l\begin{pmatrix} 1 & 0 \\ 0 & 1 \end{pmatrix}$
L_4^-	$\|1\rangle = \begin{pmatrix} 3m-1 \\ 3m+1 \end{pmatrix}$	$(-1)^{3m}\begin{pmatrix} 0 & -i \\ i & 0 \end{pmatrix}$	$-(-1)^l\begin{pmatrix} 1 & 0 \\ 0 & 1 \end{pmatrix}$
L_5^-	$\|1\rangle = \begin{pmatrix} 3m-1 \\ 3m+1 \end{pmatrix}$	$-(-1)^{3m}\begin{pmatrix} 0 & -i \\ i & 0 \end{pmatrix}$	$-(-1)^l\begin{pmatrix} 1 & 0 \\ 0 & 1 \end{pmatrix}$
L_6^+	$\|1\rangle = \begin{pmatrix} 3m \\ 3m+1 \end{pmatrix}$ $\|2\rangle = \begin{pmatrix} 3m-1 \\ 3m \end{pmatrix}$	$(-1)^{3m}\begin{pmatrix} 0 & 0 & 0 & 1 \\ 0 & 0 & 1 & 0 \\ 0 & 1 & 0 & 0 \\ 1 & 0 & 0 & 0 \end{pmatrix}$	$(-1)^{3m}\begin{pmatrix} 1 & 0 & 0 & 0 \\ 0 & -1 & 0 & 0 \\ 0 & 0 & -1 & 0 \\ 0 & 0 & 0 & 1 \end{pmatrix}$
L_6^-	$\|1\rangle = \begin{pmatrix} 3m \\ 3m+1 \end{pmatrix}$ $\|2\rangle = \begin{pmatrix} 3m-1 \\ 3m \end{pmatrix}$	$(-1)^{3m}\begin{pmatrix} 0 & 0 & 0 & 1 \\ 0 & 0 & 1 & 0 \\ 0 & 1 & 0 & 0 \\ 1 & 0 & 0 & 0 \end{pmatrix}$	$-(-1)^{3m}\begin{pmatrix} 1 & 0 & 0 & 0 \\ 0 & -1 & 0 & 0 \\ 0 & 0 & -1 & 0 \\ 0 & 0 & 0 & 1 \end{pmatrix}$

[a] $m = 0, \pm 1, \pm 2, \ldots$.

[b] see table 2 for the definition of $\hat{\pi}_l$.

[c] $\begin{pmatrix} U_l(g,-z') \\ V_l(g,-z') \end{pmatrix} \equiv \hat{\pi}_z \begin{pmatrix} U_l(g,z') \\ V_l(g,z') \end{pmatrix}$ or $\begin{pmatrix} U_l(g,-z') \\ V_l(g,-z') \\ W_l(g,-z') \\ X_l(g,-z') \end{pmatrix} \equiv \hat{\pi}_z \begin{pmatrix} U_l(g,z') \\ V_l(g,z') \\ W_l(g,z') \\ X_l(g,z') \end{pmatrix}$.

By the same token, the spin representations Λ_4, Λ_5 result from lifting the degeneracy of the zero-spin Λ_3 representation. A similar comparison at the L-point between table 3 and table 3 in I implies that the SO interaction admixes the L_1, L_2 and L_3 representations (and the negative z-parity representations L_1', L_2' and L_3') to form the spin representation L_6^+ (and L_6^-). Likewise, the $L_{4,5}^+$ spin representations (and $L_{4,5}^-$) are obtained by lifting the degeneracies in the L_3 (and L_3') zero-spin representation.

4. The multipole wavefunction

To derive the multipole wave equation we start from the Schrödinger equation in the primed coordinates [7]:

$$[-\nabla'^2 + (2m_0/\hbar^2)E_n(k) - (2m_0/\hbar^2)v(r') - (2m_0/\hbar^2)(V_{SO}(r'))](\Psi_{nk}(r')) = 0 \qquad (4.1)$$

where $v(r')$ is the central potential, $(\hat{V}_{SO}(r'))$ is the non-scalar SO interaction (2.6) and m_0 is the effective mass, chosen here [1] as the free electron mass. Inserting wavefunction and potential multipole expansions (2.5), (2.6), (2.8), and (2.7) of I, into (4.1), projecting on $e^{il\phi}$, factoring out the Bessel functions, expressing the products '$v(r')\Psi(r')$' and '$(\hat{V}_{SO}(r')\Psi(r'))$' in terms of the multipoles and projecting on the two spin states $\chi'(\sigma)$

yields the multipole wave equation [7]:

$$\left[-g_0^2+\frac{2m_0}{\hbar^2}E_n(k)+\frac{\mathrm{d}^2}{\mathrm{d}z'^2}\right]\begin{pmatrix}\Psi_l^{(1)}(g,z')\\ \Psi_l^{(-1)}(g_0,z')\end{pmatrix}+\sum_{g_P,g_F}\sum_{m=-2}^{3}A_{l,m}(g_0,g_P,g_F)$$
$$\times\left\{-\frac{2m_0}{\hbar^2}\begin{pmatrix}v_m(g_P,z') & 0\\ 0 & v_m(g_P,z')\end{pmatrix}\begin{pmatrix}\Psi_{l-m}^{(1)}(g_F,z')\\ \Psi_{l-m}^{(-1)}(g_F,z')\end{pmatrix}\right.$$
$$-\frac{2m_0}{\hbar^2}\begin{pmatrix}0 & f_m^{(-)}(g_P,z')\\ -f_m^{(+)}(g_P,z') & 0\end{pmatrix}\begin{pmatrix}\frac{\mathrm{d}}{\mathrm{d}z'}\Psi_{l-m}^{(1)}(g_F,z')\\ \frac{\mathrm{d}}{\mathrm{d}z'}\Psi_{l-m}^{(-1)}(g_F,z')\end{pmatrix}$$
$$-\frac{2m_0}{\hbar^2}\frac{g_F}{2}\begin{pmatrix}f_m^{(-)}(g_P,z') & 0\\ -2f_m^{(z')}(g_P,z') & -f_m^{(-)}(g_P,z')\end{pmatrix}\begin{pmatrix}\Psi_{l-m-1}^{(1)}(g_F,z')\\ \Psi_{l-m-1}^{(-1)}(g_F,z')\end{pmatrix}$$
$$\left.-\frac{2m_0}{\hbar^2}\frac{g_F}{2}\begin{pmatrix}f_m^{(+)}(g_P,z') & -2f_m^{(z')}(g_P,z')\\ 0 & f_m^{(+)}(g_P,z')\end{pmatrix}\begin{pmatrix}\Psi_{l-m+1}^{(1)}(g_F,z')\\ \Psi_{l-m+1}^{(-1)}(g_F,z')\end{pmatrix}\right\}=0 \quad (4.2a)$$

where

$$f_l^{(\pm)}(g_P,z')=f_l^{(x')}(g_P,z')\pm\mathrm{i}f_l^{(y')}(g_P,z'). \quad (4.2b)$$

The symbols in (4.2) are as follows. The band energy is denoted by $E_n(k')$, $\Psi_l^{(\pm1)}(g_F,z')$ are the multipoles of the two spin-projection wavefunction components (2.5), $v_m(g_P,z')$ are the central potential multipoles [1], $f_m^{(\pm)}(g_P,z')$ and $f_m^{(z')}(g_P,z')$ are the SO vector form factor multipoles given by (2.8) and (4.2*b*) and the geometrical '*A*-coefficients' $A_{l,m}(g_0,g_P,g_F)$ have been introduced and discussed in I. The wavefunction multipoles obey the Bloch theorem in the [111] direction [1]:

$$\Psi_l^{(\sigma)}(g_F,z'+a^*)=\mathrm{e}^{\mathrm{i}k'a^*}\Psi_l^{(\sigma)}(g_F,z') \quad (4.2c)$$

where k' and a^* are defined in (2.4). The Bloch theorem in the x' and y' directions is manifested in the multipole phase relations (3.1) and (3.2).

The single-variable wave equation set (4.2) is the central result of this work. It applies to the [111] direction of cubic lattices through the particular *A*-coefficients, the *l*-sequence and the *g*-sequence. In keeping with the paradigm of I, the band symmetry is specified by specifying the *l*-sequence according to tables 2 and 3, and the pertaining ascending *g*-sequence is selected from table 1 according to convergence considerations.

The first two terms in (4.2) are precisely the zero-SO wavefunction of I, but with the spin degeneracy explicitly manifested by having $\Psi^{(1)}$ and $\Psi^{(-1)}$ satisfy the same wave equation. The rest of the terms in (4.2) are SO terms. They are seen to be both diagonal and non-diagonal in σ and since the SO interaction is velocity dependent, all SO terms have either an explicit 'g_F'-factor or a first-derivative operator 'd/dz''. The complexity of (4.2) in comparison with its zero-spin counterpart (the first two terms) underscores the well known difficulty of incorporating SO interaction into band calculations. The structure of (4.2), however, implies that in the present framework the extra effort amounts to essentially just doubling the multipole basis.

The σ block structure of (4.2) for the [111] direction and a cubic lattice is given in table 4. Part (*a*) of table 4 shows that for the $L_6^{\pm}$ (Λ_6) bands the SO terms enter in one diagonal block ($l=3m+1$) and the off-diagonal blocks. By contrast, part (*b*) shows that for the $L_{4,5}^{\pm}$ ($\Lambda_{4,5}$) bands only the diagonal blocks ($l=3m\pm1$) involve SO terms. This structure is understandable. Since the $l=3m$ block is associated with s waves (and higher even *l*-waves) and the $l=3m\pm1$ blocks are associated with p waves (and higher odd *l*-waves), it follows that the diagonal $l=3m\pm1$ SO terms describe the p-wave SO interaction, while off-diagonal terms describe the SO s–p mixing. This particular structure motivates the SO parameterization adopted in section 5.

Table 4. The block structure of the wavefunctions (4.2) for the $L_6^{\pm}$ (Λ_6) and $L_{4,5}^{\pm}$ ($\Lambda_{4,5}$) bands. The corresponding σ and l-sequences are indicated.

(*a*) $L_6^{\pm}$ (Λ_6) representations

	$\sigma=-1$ $(3m+1)$	$\sigma=+1$ $(3m)$
$\sigma=-1$ $(3m+1)$	$v(g_P,z')+f^{(\pm)}(g_P,z')$	$f^{(\pm)}(g_P,z')\frac{d}{dz'}+f^{(z')}(g_P,z')$
$\sigma=+1$ $(3m)$	$f^{(\pm)}(g_P,z')\frac{d}{dz'}+f^{(z')}(g_P,z')$	$v(g_P,z')$

(*b*) $L_{4,5}^{\pm}$ ($\Lambda_{4,5}$) representations

	$\sigma=-1$ $(3m+1)$	$\sigma=+1$ $(3m-1)$
$\sigma=-1$ $(3m+1)$	$v(g_P,z')+f^{(\pm)}(g_P,z')$	0
$\sigma=+1$ $(3m-1)$	0	$v(g_P,z')+f^{(\mp)}(g_P,z')$

5. Band structure of PbSe in the Γ–L ([111]) direction

To demonstrate the implementation of (4.2) we calculate below the low bands of PbSe along the Γ–L line. This same example has been calculated and discussed in I in the absence of the SO interaction. The goal here is to compare the results with SO to other pseudopotential calculations. All of the results were obtained using a PC 386/25 MHz with 4 Mb memory in double precision. The latter is needed given the expected small band gap [2]. The secular equation in a plane wave basis employed 15 plane waves per multipole [7].

The steps in setting up the calculation are as follows [1]. First establish which bands are coupled by virtue of symmetry, then specify the phenomenological interaction and finally select the multipole basis. As table 4 shows, the $L_6^{\pm}$ (Λ_6) and $L_{4,5}^{\pm}$ ($\Lambda_{4,5}$) bands decouple, and hence are calculated separately. The central pseudopotential is taken from [13], as in I. The SO parameterization, however, is not readily available: [12] and [13] incorporate the SO interaction using different formalisms, with parameters not explicitly given. Therefore we are led to adopt a parameterization compatible with (2.7) and based on a mix of atomic and measured band structure data [12–15]. Thus for PbSe with two atoms in the unit cell, we assume two local SO form factors $\zeta_{Pb}(|r-r_{Pb}|)$, $\zeta_{Se}(|r-r_{Se}|)$ (r_{Pb} at the origin and r_{Se} at $r_{Se}=(0,0,a^*/2)$ of the unit cell) with a normalized Gaussian radial dependence [7]. This choice calls for four parameters: the two strengths and two ranges of the $\zeta(|r|)$ form factors. For the ranges we take the atomic core radii $r(\mathrm{Pb})=1.45$ Å and $r(\mathrm{Se})=1.16$ Å. The form factor strengths are parameterized in proportion to the atomic Pb and Se SO strengths, with a ratio of four [7, 12, 14, 15]. The overall SO strengths are left as adjustable parameters, which are fitted to particular measured band gaps. To accommodate the difference between the s and p wave SO strengths [16], and based on the block structure of table 4, we introduce two dimensionless scale parameters S_D and S_{ND} for the diagonal and off-diagonal blocks of table 4, respectively. Thus the overall SO strengths for Pb and Se are $A(\mathrm{Pb})$, $A(\mathrm{Se})$ where

$$(A(\mathrm{Pb}))=\begin{pmatrix}S_D\\S_{ND}\end{pmatrix}\lambda(\mathrm{Pb})\qquad(A(\mathrm{Se}))=\begin{pmatrix}S_D\\S_{ND}\end{pmatrix}\lambda(\mathrm{Se}) \tag{5.1}$$

and $\lambda(\mathrm{Pb})$, $\lambda(\mathrm{Se})$ are atomic SO strengths chosen as $\lambda(\mathrm{Pb})=0.56$ eV and $\lambda(\mathrm{Se})=0.14$ eV [7].

The last step is choosing the multipole basis set. Recalling that the SO interaction is the non-scalar relativistic *correction* to the central pseudopotential (although it may substantially alter specific bands) the natural choice is the set for which the central pseudopotential calculations converge. For the $L_6^{\pm}$ bands, table 5 in I and table 4 indicate that this set is comprised of 12 multipoles, the six multipoles for the L_3, L_3' bands and the six multipoles for the L_1, L_2' bands, all admixed by the SO interaction. Correspondingly, the $L_{4,5}^{\pm}$ bands employ the six multipoles for the L_3, L_3' bands [1]. Unfortunately, the largest set that can be handled by our computer is eight multipoles. Consequently, for the $L_6^{\pm}$ bands we choose (table 5 in I, table 4) the following. For $\sigma = -1$ the multipoles are $(l, g(n)) = (-2, g(2))$, $(1, g(2))$, $(-2, g(3))$, $(1, g(3))$ and for $\sigma = 1$ they are $(l, g(n)) = (0, g(1))$, $(0, g(2))$, $(0, g(3))$, $(3, g(2))$, where $g(n)$, in ascending order, are listed in table 1. Correspondingly, the set for the $L_{4,5}^{\pm}$ bands is (see table 4) $(l, g(n)) = (-2, g(2))$, $(1, g(2))$, $(-2, g(3))$, $(1, g(3))$ for $\sigma = \pm 1$. However, this multipole basis has two drawbacks: as figure 1(*a*) shows, it is *not* adequate for the lower half of the Γ–L line as evidenced by the band crossings for $K \leqslant 0.5$ (2.4). Also, the calculated L-point band gap is considerably larger than the experimental value, i.e., 0.53 eV versus 0.16 eV [2]. Notwithstanding these disadvantages, for the present purpose of demonstrating the implementation and validity of (4.2) this set is appropriate. In particular, the physically interesting band structure around the L point ($K = 1$) is well within the convergence domain, and the effect of the large zero-SO band gap is expected just to be reflected in 'large' fitted SO strengths.

Table 5. The qualitative dependence of the relevant $L_6^{\pm}$ band energies (eV) near the band gap in PbSe on the two SO strength parameters, (5.1). The eight-multipole set discussed in section 5 that enters the calculation is as follows. For $\sigma = -1$ the multipoles are $(l, g(n)) = (-2, g(2))$, $(1, g(2))$, $(-2, g(3))$, $(1, g(3))$ and for $\sigma = 1$ they are $(l, g(n)) = (0, g(1))$, $(0, g(2))$, $(0, g(3))$, $(3, g(2))$ and $g(n)$, in ascending order, are listed in table 1. The arrow indicates the band energy movement with respect to the zero-SO bands. The band gap ΔE is between the two innermost bands.

	S_{ND}, S_D					
Band symmetry	0, 0	0, −20	0, 20	±30, 0	30, 30	−30, −30
L_6^-	(L_3') 10.7	11.4 ↑	10.0 ↓	10.6 ↑	10.0 ↓	11.7 ↑
L_6^-	(L_2') 9.4	9.4	9.4	9.3 ↓	9.4 ↑	9.3 ↓
L_6^+	(L_1) 8.9	8.9	8.9	8.8 ↓	9.1 ↑	8.8 ↓
L_6^+	(L_3) 7.2	6.8 ↓	7.5 ↑	7.0 ↓	7.5 ↑	6.5 ↓
$\Delta E(L_6^- - L_6^+)$	0.5	0.5	0.5	0.5	0.3	0.5

Before presenting the full calculation, the qualitative SO features for the four relevant $L_6^{\pm}$ bands around the band gap are demonstrated in table 5. Again, in the absence of SO interaction these bands are depicted in figure 1(*a*) [1]. In the presence of the SO interaction consider first the limit of $S_{ND} = 0$. As table 4 implies, only the p-wave blocks ($l = 3m + 1$) are modified. This is evident from the second and third columns of table 5: the outermost two $L_6^{\pm}$ bands, which pertain to the p-like L_3, L_3' components, move, while the innermost two $L_6^{\pm}$ bands, which pertain to the s-like L_1, L_2' components, do not. This l-assignment is consistent with the known angular momentum content of these bands [17, table IV]. Note that positive S_D leads to band clustering while negative S_D has the opposite effect. In the other limit of $S_D = 0$, table 4 implies that only off-diagonal s–p mixing blocks do not vanish. As the fourth column in table 5 shows, the band gap is reduced in this case regardless of the sign of S_{ND}. This result is plausible in view of the compatibility relations

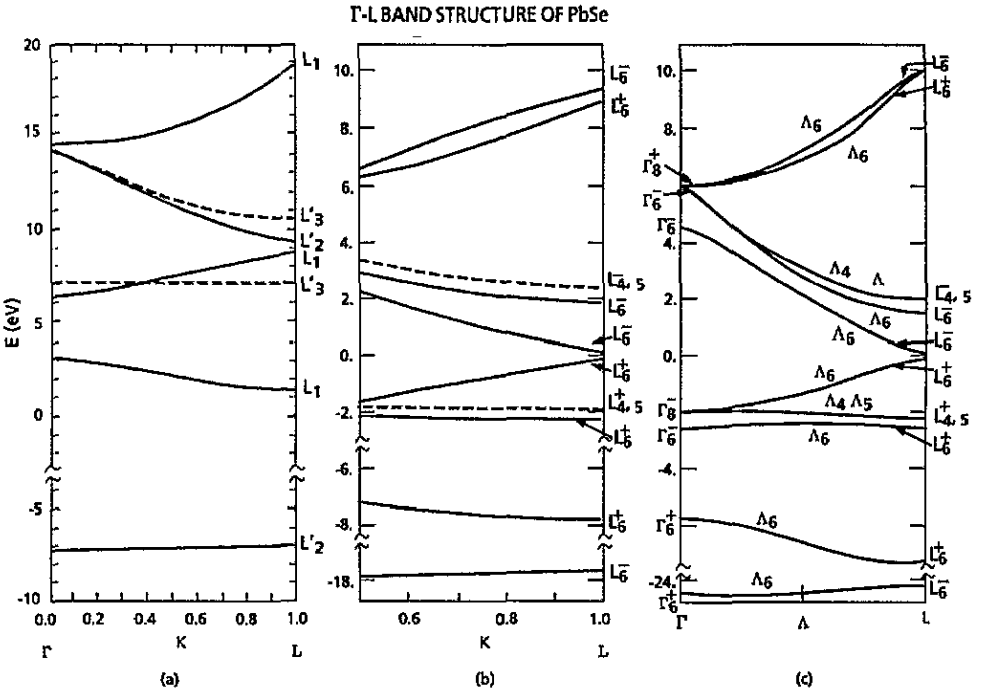

Figure 1. Calculated band structures of PbSe along the Γ–L direction. Band symmetries are denoted in the notation of [10]. (*a*) The zero-SO band structure interaction. The (L_1, L_2') and (L_3, L_3') bands are each calculated with their four-multipole basis discussed in section 5 [1, table 5]. The K symbol is defined in (2.4). (*b*) The calculated band structure for $K \geqslant 0.5$ with SO strength parameters (5.1) $S_D = -15$, $S_{ND} = -60$. The multipole basis employed for the $L_6^{\pm}$ bands is the eight-multipole basis discussed in section 5 and mentioned in the caption to table 5. The $L_{4,5}^{\pm}$ bands are calculated with the four multipoles discussed in section 5. (*c*) The [11] band structure reproduced from [13].

discussion in section 3: the SO interaction admixes the (L_3, L_1) and the (L_3', L_2') bands. Consequently, given the particular arrangement of the L_3, L_1, L_2', L_3' bands around the band gap in figure 1(*a*) a level-repulsion argument implies that the innermost band gap is reduced by the SO interaction. This qualitative trend is clearly demonstrated in figure 2(*a*) for the particular case of $S_D = S_{ND} < 0$.

When S_{ND}, $S_D \neq 0$, the 'correct' signs of S_D, S_{ND} are assessed by the following consideration. For the $L_6^{\pm}$ bands (table 4), which determine the band gap, the difference between the diagonal 'v' terms (the $l = 3m$ block) and the '$v + f^{\pm}$' terms (the $l = 3m \pm 1$ block) corresponds to the difference between the $s_{1/2}$ and $p_{1/2}$ SO potentials. Since for the related semiconductor PbTe this difference is negative [16], it is expected that $S_D < 0$. The S_{ND} parameter is expected to have the same sign since the symmetries of (4.2), which was derived assuming $S_{ND} = S_D$, are preserved only when S_D and S_{ND} have the same sign. Indeed, as the last two columns of table 5 show, taking S_D and $S_{ND} > 0$ leads to 'clustering' of all four bands, which is inconsistent with another band structure calculation [13] (figure 1(*c*)). Therefore that the physical choice is S_D and $S_{ND} < 0$, in keeping with the argument above. For this sign choice, figure 2(*b*) shows that a sufficiently strong SO interaction reduces the band gap to the point of 'band inversion' and beyond. This effect underlies the observed 'inverted gaps' in heavy-element narrow-gap semiconductors, such

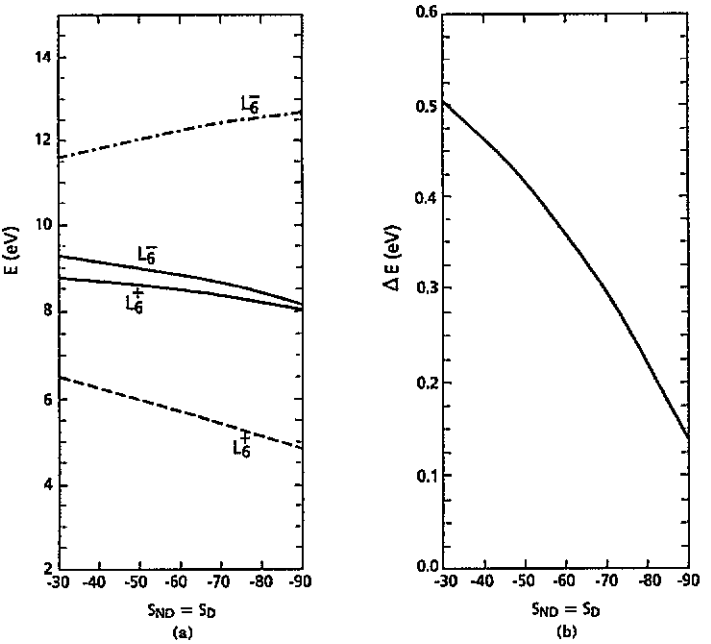

Figure 2. The dependence of the relevant $L_6^{\pm}$ bands near the band gap on the SO strength parameters for $S_D = S_{ND} < 0$: (*a*) the four nearest bands; (*b*) the corresponding band gap ΔE.

as in the IV–VI system [2].

Figure 1(*b*) and 1(*c*) compares the calculated ten lowest bands for $K \geqslant 0.5$ and a 'correct' band structure. For the latter we take the calculation of Kohn *et al* [13] given that other pseudopotential and *ab initio* calculations [12, 13, 16, 17] yield essentially identical results near the band gap. The comparison for the relevant six bands near the band gap is seen to be good. The fitted SO parameters $S_D = -15$, $S_{ND} = -60$ approximately reproduce three experimental band gaps at the L-point: the band gap $E(L_6^-) - E(L_6^+) = 0.24$ eV and the gaps between the two adjacent L_6^+ and L_6^- bands, which are 1.86 eV and 2.14 eV, respectively. These band gaps are in good agreement with the calculations of Kohn *et al* [13]. The fitted SO strengths reflect the fact that the zero-SO band gap (0.53 eV [1]) is larger than the experimental value by about a factor of four. The value of S_D is of the correct magnitude since $S_D/4$ yields strengths A(Pb), A(Se) (5.1) comparable to atomic SO splittings [14]. For $K \leqslant 0.5$, where the present zero-spin multipole set is inadequate (see figure 1(*a*)), the calculated band structure is expected to give poor results since the SO interaction—which is but a correction to the central potential—cannot compensate for inadequacies in the central potential band description.

In summary, we have generalized a cylindrical coordinate method for local pseudopotential band calculations to include spin degrees of freedom and the SO interaction. The ensuing set of coupled, one-dimensional wave equations is derived. Their implementation is demonstrated for the test case of PbSe bandstructure in the [111] direction. These results establish the usefulness of the generalized cylindrical multipole expansion method with the following proviso: provided the chosen basis adequately describes the central pseudopotential band structure in a portion of the Brillouin zone. The reverse is also true: whenever the chosen multipole basis inadequately describes the central potential bandstructure, adding the SO correction is expected to produce unphysical results. Another

attractive feature of the cylindrical representation is that it indentifies the band admixtures which are induced by the SO interaction. In the particular case of PbSe (and the Pb salts), the tendency toward band inversion for a sufficiently strong SO interaction can be readily understood.

Acknowledgments

We would like to acknowledge useful discussions with Dr J R Cullen. This work was supported by the Office of Naval Research and the NSWC Independent Research Funds.

References

[1] Agassi D and Restorff J B 1994 *J. Phys.: Condens. Matter* **6** 1497
[2] Nimtz G and Schlicht B 1985 *Narrow Gap Semiconductors (Springer Tracts in Modern Physics 98)* (Berlin: Springer); 1962 *Physics and Chemistry of II–VI Compounds* ed M Aven and J S Prener (Amsterdam: North-Holland)
[3] See, for instance, Philips J C 1973 *Bonds and Bands in Semiconductors* (New York: Academic) p 122
[4] Erickson R P, Hathaway K B and Cullen J R 1993 *Phys. Rev.* B **47** 2626 and references therein
[5] See, for instance, Cohen M H and Blount E I 1960 *Phil. Mag.* **5** 115
Yaffet Y 1963 *Solid State Physics* vol 13, ed F Seitz, D Turnbull (New York: Academic) p 2
[6] Abramowitz M and Stegun I A 1964 *Handbook of Mathematical Functions (Applied Mathematics Series 55)* (Washington, DC: National Bureau of Standards) ch 9
[7] Agassi D and Restorff J B *NSWC Technical Report* TR91-326 available upon request from the National Technical Information Service, Springfield, VA 22161
[8] See, for instance, Zeiger H J and Pratt G W 1973 *Magnetic Interactions in Solids* (Oxford: Clarendon) appendix 4
[9] Morgan D J 1965 *Solid State Theory* ed P T Landsberg (London: Wiley–Interscience) p 232
[10] Slater J C 1965 *Quantum Theory of Molecules and Solids* vol 2 (New York: McGraw-Hill) appendix 9
[11] Jones H 1975 *The Theory of Brillouin Zones and Electronic States in Crystals* 2nd edn (Amsterdam: North-Holland) ch 7
[12] Martinez G, Schluter M and Cohen M L 1975 *Phys. Rev.* **11** 651
[13] Kohn S E, Yu R Y, Petroff Y, Shen Y R, Tsang Y and Cohen M L 1973 *Phys. Rev.* B **8** 1477
[14] Philips J C 1973 *Bonds and Bands in Semiconductors* (New York: Academic) p 178
[15] Zeiger H J and Pratt G W 1973 *Magnetic Interactions in Solids* (Oxford: Clarendon) p 85
[16] See, Rabe K M and Joannopoulos J D 1985 *Phys. Rev.* **32** 2303; PbTe and PbSe belong to the same IV–VI system
[17] Dalven R 1973 *Solid State Physics* vol 28, ed Ehrenreich H, Seitz F and Turnbull D (New York: Academic) p 179